June 1987 LRP 326/87

Finite Element Methods Applied to Radiofrequency Waves

L. Villard

External Kink Imposed Operating Boundaries in Tokamaks

W.A. Cooper, F. Yasseen, F. Troyon, T. Tsunematsu and A.D. Turnbull

Lectures presented at the

Spring College On Plasma Physics

Trieste, Italy

May 25 - June 19, 1987

Lecture Notes

FINITE ELEMENT METHODS APPLIED TO RADIOFREQUENCY WAVES

L. Villard

Centre de Recherches en Physique des Plasmas
Association Euratom - Confédération Suisse
Ecole Polytechnique Fédérale de Lausanne
21, Av. des Bains, CH-1007 Lausanne/Switzerland

ABSTRACT

The study of radiofrequency (rf) waves is one of the oldest [1-3] and most fertile field of research in plasma physics. In this lecture we shall point out the problem of wave propagation and absorption in connection with rf heating of magnetized plasmas.

We shall survey the numerical techniques to solve relevant differential equations, in particular the finite element methods [4] which are so universal that they are applied to numerous other problems in physics and engineering: aerodynamics, elasticity theory, solid state physics. etc.

In the first part of this lecture these methods are presented. As a particular example we have chosen the cold plasma wave equation in one-dimensional (1-D) geometry. We outline how the finite element methods are applicable to time-dependent and/or non-linear equations, such as Fokker-Planck or quasi-linear equations.

The second part of this lecture is dedicated to the cold and warm plasma wave propagation and absorption in toroidal geometry in the Alfvén Wave and Ion Cyclotron Range of Frequency (AWRF and ICRF, respectively). After derivation of the basic equations in exact geometry we apply the discretization procedure described in the first part, but there in a two-dimensional (2-D) domain. Some results are presented and discussed. In particular the physics of 2-D resonance absorption and the presence of global modes are analyzed.

I. INTRODUCTION

A complete presentation of the physics of rf heating in magnetized plasmas is certainly beyond the scope of this lecture. We merely show guidelines to the problems and in particular what has been called the "global wave" approach. The subject is presented in such a way that the methods of resolution can be generalized to other problems. By "global" approach we mean the global determination of the wave field in non-homogeneous, non-uniformly magnetized, finite size plasmas. We emphasize two points here: Firstly, the problem is solved in one well-defined geometry, in the whole domain (plasma, vacuum, antenna and shell) and, secondly, the solution obtained is by essence the sum of all incident, transmitted, reflected and evanescent waves.

In the AWRF and ICRF, three basic physical phenomena can be exploited for rf heating:

1) The existence of global eigenmodes of the fast magnetosonic wave and of the Alfvén (or ion-cyclotron) wave.

2) The perpendicular resonances of the cold plasma model, Alfvén and ion-ion hybrid, which are described in hot plasma theory as mode conversion points ("mode conversion regime").

3) The ion cyclotron damping, which can be exploited in two ways: either by adding a small fraction of another ion species ("minority regime") or by setting the frequency equal to a harmonic of the ion cyclotron frequency ("harmonic regime").

The first problem to tackle is the choice of a physical model. Depending on its sophistication the description of the above-mentioned phenomena will be more or less complete (provided that the equations can be solved!). It can be said that the finer the model, the more difficult it is to solve exactly. The skill of the physicist consists of finding a model giving a good description of the basic phenomena (1^o, 2^o and 3^o) together with an accurate method of resolution. A sophisticated model resolved with such or such approximation may give results of weaker physical contents than a rougher model solved exactly.

For our problem of waves in plasmas there exist different models, named "cold", "warm" or "hot" plasma, depending on the degree at which we take into account the effect of the temperature on the waves and their damping. We have also the alternative of neglecting the electron inertia, an approximation which is often made in the AWRF and ICRF. These different models describe different waves and different absorption mechanisms. The reader can refer to Table I for a summarized comparison between these models.

Another difficulty is related to the complexity of the geometry of the magnetic configuration. See Fig. 1 for the tokamak case. Some authors use a 1-D approximation (plane or cylinder), or make a development in inverse aspect ratio [5]. Some neglect the poloidal magnetic field. Some authors use different geometrical approximations in different parts of the plasma [6,7]. We shall demonstrate how the "exact" geometry of the ideal MHD equilibrium can be taken into account in Chapter 3.

The next problem to treat is the inhomogeneity of the plasma. It is crucial to describe it since much of the physics (mode conversion, resonance absorption, accessibility, etc.) depends on it. A possible approximation is the geometrical optics approximation, or "WKB" (Wentzel, Kramers, Brillouin). It consists of defining a local wavelength and assume that the properties of the substance do not vary too much on a wavelength. Unfortunately, its limitations are numerous. In the AWRF the wavelengths are larger than the dimensions of the system. Moreover, WKB is not valid near the most interesting points: the resonances, where the WKB-defined wavelength becomes infinite; the mode conversion points, where two wavebranches come close to each other; or the places where strong absorption occurs, such as the vicinity of the ion cyclotron frequencies or their harmonics. Therefore, the models based on WKB approximation must be coupled to other methods such as the use of an analytical formula near the resonances. However, the use of WKB approximation is not compulsory and in Chapter 2 we shall present how we can solve the equations without any WKB-type of approximation.

Moreover, the plasmas that one wishes to study are bounded. Many models ignore it and can only compute the "single-pass absorption" but not the total wavefield consisting of all incident transmitted, reflected and evanescent waves. It is only in taking into account the finite size of the plasma, with

appropriate boundary conditions, that the global eigenmodes or global oscillations of the plasma column can be described.

The necessary tool for the resolution of the equations remains to be defined. There are mainly two "philosophies": the methods based on the WKB approximations (ray tracing [8] for example) and the "global wave" methods (finite differences [5] at finite elements [9]), though there are intermediate approaches such as the parabolic approximation [10]. Actually only the finite element methods can fully take into account the complexity of the geometry, the inhomogeneity, and the finite size of the plasmas. They have a sound mathematical foundation [4] and have been since a long time applied to other domains of physics: elasticity theory, aerodynamics, hydrodynamics, thermodynamics, etc. Their application to the problem of rf heating is rather recent. The aim of this lecture is to show their pertinence and to demonstrate that they are powerful and useful tools for the investigation of physical processes.

Chapter 2 presents the finite element methods on a simple example. Chapter 3 deals with an application to rf heating in the AWRF and ICRF in toroidal geometry [9,11,12].

II. NUMERICAL TECHNIQUES BASED ON THE FINITE ELEMENT METHODS

We assume that we have chosen a physical model and a given geometry, and that we have obtained a system of ordinary or partial differential equations (ODE or PDE) for our problem. In this chapter, we shall not make the derivation of these equations but introduce the finite element method on a simple 1-D equation:

$$-\frac{d}{dx}\left(\alpha(x)\frac{dE}{dx}\right) + \beta(x)E = f(x), \quad x \in \Omega=[0,1], \tag{2.1}$$

where $\alpha(x)$, $\beta(x)$ and $f(x)$ are given sufficiently smooth functions. We impose Dirichlet boundary conditions:

$$\begin{cases} E(0) = a & (2.2a) \\ E(1) = b & (2.2b) \end{cases}$$

We simply mention here that Eq. (2.1) has the structure of the wave equation of the cold plasma model with $E_{\parallel} = 0$ (model 1 of Table I) in a plane geometry. The inhomogeneity is along x-axis, the magnetic field is parallel to the z-direction and in this case E is the y-component of the wave electric field [13].

The first step to solve (2.1) (2.2) with the finite element method is to obtain a variational form of the equation. This can be easily done in the following way:

1° Multiply (2.1) with a sufficiently regular test-function $\tilde{E}(x)$ such that $\tilde{E}(o) = \tilde{E}(1) = 0$.

2° Integrate over the domain where the solution is searched :

$$\int_0^1 \left(\tilde{E} \frac{d}{dx} \left(-\alpha \frac{dE}{dx} \right) + \tilde{E} \beta E \right) dx = \int_0^1 \tilde{E} f \, dx \, .$$

3° Integrate by parts

$$\int_0^1 \left(\alpha \frac{d\tilde{E}}{dx} \frac{dE}{dx} + \beta \tilde{E} E \right) dx = \int_0^1 \tilde{E} f dx \, . \qquad (2.3)$$

We can now formulate the problem variationally: "find E(x) in [0.1] such that (2.3) is satisfied for any test-function $\tilde{E}(x)$". This problem is equivalent to finding a solution of (2.1), except that the solution of (2.3) has less restrictions on its smoothness: the integration by parts has lowered the order of the highest derivative operating on E.

The second step is to discretize the domain [0,1] into a finite number of intervals $\{x_i, i = 0..N, x_o = 0, x_N = 1\}$. The intervals need not to have all the same size.

The third step is the heart of the finite element methods: we approximate the unknown function E(x) and the test-function $\tilde{E}(x)$ by piecewise polynomials (see Fig. 2). In other words, we expand the function E in a basis of functions $\phi i(x)$ having a finite support :

$$E(x) = \sum_{i=0}^{N} v_i \phi_i(x) \quad , \tag{2.4a}$$

and usually we use the same basis of functions for the test-function:

$$\tilde{E}(x) = \sum_{j=0}^{N} w_j \phi_j(x) \quad . \tag{2.4b}$$

The functions $\phi_i(x)$ have the property $\phi_i(x_j) = \delta_{ij}$. Figure 2 shows the example of linear elements. The coefficients v_i become now the unknowns of the problem.

The fourth step is to introduce the Ansatz (2.4) into the variational form (2.3). The discretized problem can then be formulated: "find $\{v_i, i = 0..N\}$ such that

$$\int_0^1 \left\{ \alpha \left(\sum_{j=0}^{N} w_j \phi_j' \right)\left(\sum_{i=0}^{N} v_i \phi_i' \right) + \beta \left(\sum_{j=0}^{N} w_j \phi_j \right)\left(\sum_{i=0}^{N} v_i \phi_i \right) \right\} dx$$

$$= \int_0^1 f \left(\sum_{j=0}^{N} w_j \phi_j \right) dx \quad ,$$

$$\forall \{ w_j , j = 0..N \} \text{"} . \tag{2.5}$$

The prime denotes the derivative with respect to x. Let us define

$$A_{ij} = \int_0^1 \{ \alpha \phi_i' \phi_j' + \beta \phi_i \phi_j \} dx \quad , \tag{2.6}$$

$$b_i = \int_0^1 f \phi_i \, dx \quad , \tag{2.7}$$

and the vectors $\underline{v} = (v_0, v_1, \ldots, v_N)$, $\underline{w} = (w_0\ w_1, \ldots, w_N)$, $\underline{b} = (b_0, b_1, \ldots, b_N)$. With (2.6) and (2.7), the problem (2.5) is equivalent to "find $\underline{v} \in \mathbb{R}^{N+1}$ such that

$$\underline{w} \cdot A\underline{v} = \underline{w} \cdot \underline{b} \quad , \forall\, \underline{w} \in \mathbb{R}^{N+1} \; ; \tag{2.8}$$

or "find $\underline{v} \in \mathbb{R}^{N+1}$ such that

$$A\ \underline{v} = \underline{b} \tag{2.9}$$

Note that we have to introduce the boundary conditions (2.2). Those imply that $v_0 = a$ and $v_N = b$. In other words we must set

$$\begin{aligned} A_{00} &= \frac{b_0}{a} \quad , \quad A_{0j} = 0 \ \forall j > 0 \quad , \\ A_{NN} &= \frac{b_N}{b} \quad , \quad A_{Nj} = 0 \ \forall j < N \quad . \end{aligned} \tag{2.10}$$

Suppose that the boundary condition at x = 1, E(1) = b is replaced by the condition

$$E'(1) + c_1 E(1) = d_1 \quad , \tag{2.11}$$

where c_1 and d_1 are given. This type of boundary condition arises quite often, for example in our problem of rf waves. It is called a natural boundary condition because it appears in a natural way in the variational form. (The condition (2.2) is called an essential boundary condition because it has to be explicitely and a posteriori imposed on the matrix A.) Let us consider our new problem, namely Eq. (2.1) together with the boundary conditions (2.2a) and (2.11), and let us follow the steps described before. We multiply (2.1) with $\tilde{E}(x)$ such that $\tilde{E}(0) = 0$ (but $\tilde{E}(1) \neq 0$), we integrate by parts and we get

$$\int_0^1 \left\{ \alpha \tilde{E}' E' + \beta \tilde{E} E \right\} dx - \alpha(1) \tilde{E}(1)\, E'(1) = \int_0^1 f \tilde{E}\, dx \quad .$$

We can see that the boundary condition (2.11) appears in the term integrated by parts. We can write:

$$\int_0^1 \{\alpha \tilde{E}' E' + \beta \tilde{E} E\} dx + \underbrace{c_1 \alpha(1) \tilde{E}(1) E(1)}_{(*)} = \int_0^1 f \tilde{E}\, dx + \underbrace{d_1 \alpha(1) \tilde{E}(1)}_{(**)}.$$

The boundary condition (2.11) will therefore appear as contributions to the matrix A (*) and to the source vector $\underline{b}$ (**).

Let us follow on our path. The fifth step is to choose an integration scheme for the calculation of A_{ij} and b_i, eqs. (2.6) (2.7). We note that from the definition of the basis functions, having a finite support, only a few elements of A_{ij} will be non-zero. In our case (linear elements, Fig. 2) we have $A_{ij} \neq 0$ only for $j = i-1, i, i+1$. Hence the matrix A is tridiagonal. The most rational way to construct A is to proceed interval after interval ("element by element"). Let us consider the k-th interval $\Delta_k = [x_{k-1}, x_k]$. Only the functions ϕ_{k-1} and ϕ_k will contribute to the matrix (Fig. 2). Let us define

$$\begin{cases} M_{11} = \int_{\Delta_k} (\alpha \phi'_{k-1} \phi'_{k-1} + \beta \phi_{k-1} \phi_{k-1})\, dx \\ M_{12} = \int_{\Delta_k} (\alpha \phi'_{k-1} \phi'_k + \beta \phi_{k-1} \phi_k)\, dx \\ M_{21} = M_{12} \\ M_{22} = \int_{\Delta_k} (\alpha \phi'_k \phi'_k + \beta \phi_k \phi_k)\, dx \end{cases} \qquad (2.13)$$

$$\begin{cases} S_1 = \int_{\Delta_k} f \phi_{k-1}\, dx \\ S_2 = \int_{\Delta_k} f \phi_k\, dx \end{cases} \qquad (2.14)$$

The contribution from k-th element to matrix A is the 2×2 "local matrix" M; to source vector b, it is the "local vector" (S_1, S_2). These contributions are added at the correct place by means of a correspondence between the "local numbering" (1,2) of the nodal points of Δ_k and the "global numbering" (k-1, k). Note that in this case the correspondence is trivial. More care has to be taken in the case of multi-dimensional problems or when ther are more than one unknown field.

The integrals (2.13) and (2.14) are usually computed with the Gaussian integration formulae, which express an integral over the interval $[-1,1]$ as

$$\int_{-1}^{+1} g(\xi)\, d\xi \cong \sum_{\ell=1}^{m} c_\ell\, g(\xi_\ell) \quad . \tag{2.15}$$

Table II displays the weights c_ℓ and the abcissae ξ_ℓ for the 1- to 4- point formulae. The m-point formula integrates exactly polynomials of order 2m-1. Hence the order of the error is $0(h^{2m})$. In our case ($\phi(x)$ linear), if we want to integrate exactly (2.13) for $\beta(x)$ linear, we must integrate exactly 3rd order polynomials and thus choose m = 2.

The sixth step is to solve the linear algebraic system of equations $\underline{A}\underline{v} = \underline{b}$(2.9). The safest procedure is the Gaussian elimination:

$$A = LDU \quad ; \quad LD\underline{y} = \underline{b} \quad ; \quad U\underline{v} = \underline{y} \quad , \tag{2.16}$$

where L and U are lower and upper triangular matrices and D is a diagonal matrix. We mention here that there are also iterative methods to solve $\underline{A}\underline{v} = \underline{b}$: Gauss-Seidel, Successive Over-Relaxation (SOR), Conjugate Gradients (CG), etc. Most of them are valid only for symmetric positive definite matrices. Unfortunately for our wave-propagation problem the matrices obtained are general complex matrices without any "good" property.

The seventh and last step is to reconstruct the field E(x) from the solution vector $\underline{v}$ according to (2.4a) and to make diagnostics of the solution (in our case the power flux, the power absorption, the polarizations, etc.).

How good will the solution be? In other words, for a given number of intervals N how close to the exact solution will we be? For model problems such as ours and for "good" functions $\alpha(x)$ and $\beta(x)$, one can mathematically demonstrate that the discretized solution converges towards the exact solution. The order of accuracy, $O(h^n)$, where $h = 1/N$, depends on the order of the polynomials chosen as basis functions and on the order of accuracy of the integration formula. Therefore, the basic check of the numerical procedure described above is to vary N and look whether the solution converges. This is by the way a great advantage of these methods: the accuracy of the solution can be measured.

Exercises: (1) For $\alpha(x)$ and $\beta(x)$ = const. compute the matrix elements of M (Eq. 2.13) for linear basis functions $\phi(x)$ (define $h_k = x_k - x_{k-1}$).

(2) For $h_k = h \ \forall k$ construct the matrix A.

Remark on time-dependent problems

Suppose that we want to solve an equation of the type :

$$\frac{\partial f(\underline{x}, t)}{\partial t} = (\mathcal{L} f)(\underline{x}, t) \quad , \tag{2.17}$$

where $\mathcal{L}$ is a spatial differential operator. We can straighforward apply the finite element scheme (steps 1 to 5) described above. We formally get

$$A \dot{\underline{f}} = B \underline{f} \quad , \tag{2.18}$$

where $\underline{f}$ is the vector of unknowns f_j at nodal points and the dot denotes the time derivative. We need a time-integration scheme to integrate (2.18). Let us define a discretization of the time $\{t_n\}$. At n-th timestep, $\underline{f}^{(n)}$ is known and we compute $\underline{f}^{(n+1)}$ using

$$A \left(\frac{\underline{f}^{(n+1)} - \underline{f}^{(n)}}{t^{(n+1)} - t^{(n)}} \right) = B \left(\delta \underline{f}^{(n+1)} + (1-\delta) \underline{f}^{(n)} \right) \tag{2.19}$$

with $0 \leq \delta \leq 1$. The case $\delta = 0$ is said to be an explicit scheme, $\delta = 1$ is an

implicit scheme. The case $\delta = 1/2$ is known as the Crank-Nicholson scheme. At each time step we must solve the algebraic problem:

$$(A - \delta \Delta t B)\, \underline{f}^{(n+1)} = (A + (1-\delta)\Delta t B)\, \underline{f}^{(n)}. \qquad (2.20)$$

The system (2.20) can usually be solved with iterative methods. Note that there are other integration schemes ("Alternate Direction Implicit", "Chebychev acceleration", etc.).

Remark on non-linear problems

Suppose that we want to solve an equation of the type :

$$(\mathcal{L} f)(\underline{x}) = F(f(\underline{x})) \qquad (2.21)$$

where $\mathcal{L}$ is a linear differential operator and F is a non-linear function. The simplest way to solve (2.21) is to use the iterative Picard's scheme. Suppose that we are at k-th iteration and that an approximation $f^{(k)}$ has been constructed. We compute $f^{(k+1)}$ using

$$(\mathcal{L} f^{(k+1)})(\underline{x}) = F(f^{(k)}(\underline{x})) \qquad (2.22)$$

We can solve Eq. (2.22) at each iteration step with a finite element method as depicted above. We obtain the algebraic equations

$$A\, \underline{f}^{(k+1)} = \underline{b} \qquad (2.23)$$

where A is the discretized version of $\mathcal{L}$ and $\underline{b}$ is the discretized version of $F(f^{(k)})$.

Note that to ensure that the Picard's scheme is stable one usually underrelax the new guess $\underline{f}^{(k+1)}$ of the solution:

$$\underline{f}^{(k+1)} := \omega \underline{f}^{(k+1)} + (1-\omega)\underline{f}^{(k)} \quad , \; 0 < \omega < 1 \; . \tag{2.24}$$

More sophisticated schemes are the Newton and continuation methods.

III. ALFVEN AND ICRF IN TOROIDAL GEOMETRY

III.1 Basic Equations of the Cold Plasma Model

Let us consider a magnetized multi-species plasma in an ideal MHD equilibrium state:

$$\underline{B}_o(\underline{x}) \; , \; n_{eo}(\underline{x}) \; , \; n_{io}(\underline{x}) \; , \; \underline{v}_{eo}(\underline{x}) \; , \; \underline{v}_{io}(\underline{x}) \; , \; m_i \; , \; q_i \; ; \; e n_{eo} = \sum_i n_{io} q_i \; . \tag{3.1}$$

We assume that it carries a current $\underline{j}_o$, and that this current is parallel to $\underline{B}_o$ ("force-free" condition)

$$\underline{j}_o = \mu \underline{B}_o \quad . \tag{3.2}$$

We neglect the electron inertia and assume no electric field ($\underline{E}_o = 0$) and no mass flow ($\underline{v}_{io} = 0$). This implies that the equilibrium current is carried by electrons:

$$\underline{j}_o = - e n_e \underline{v}_{eo} = - e n_e v_{eo} \underline{e}_{\parallel} \tag{3.3}$$

where $\underline{e}_{\parallel} = \underline{B}_o / B_o$.

Let us now consider a perturbation $\sim e^{-i\omega t}$ and linearize the equations of motion:

$$\begin{cases} (1) \quad 0 = \underline{E} + \underline{v}_e \times \underline{B}_o + v_{eo} \underline{e}_{\parallel} \times \underline{B} & (3.4a) \\ (2) \quad -i\omega \underline{v}_i = \dfrac{q_i}{m_i} (\underline{E} + \underline{v}_i \times \underline{B}_o) & (3.4b) \\ (3) \quad \underline{j} = \sum_i n_{io} q_i \underline{v}_i + n_{eo}(-e)\underline{v}_e & (3.4c) \\ (4) \quad \mathrm{rot}\, \underline{E} = i\omega \underline{B} & (3.4d) \\ (5) \quad \mathrm{rot}\, \underline{B} = \mu_0 \underline{j} \quad . & (3.4e) \end{cases}$$

The basic feature of the derivation is to project these eqs. in the local magnetic frame of reference, in the parallel direction to $\underline{B}_o(\underline{e}_\parallel = \underline{B}_o/B_o)$ and in the perpendicular plane to $\underline{B}_o(\underline{e}_N, \underline{e}_\perp)$. See Fig. 1 for the toroidal case.

Taking the parallel component of (3.4a), we immediately get

$$E_\parallel = 0 \tag{3.5}$$

Thus we do not need the parallel equation of motion anymore. Operating with $\underline{e}_\parallel \times$ on (3.4a) and (3.4b) and introducing into (3.4c) we obtain a relation between the perturbed current $\underline{j}$ and the wave fields $\underline{E}$ and $\underline{B}$. With Maxwell's equation (3.4d) (3.4e) we get in the $(\underline{e}_N, \underline{e}_\perp)$ coordinates:

$$\text{rot rot } \underline{E} - \underline{\underline{\varepsilon}}\, \underline{E} = 0 \tag{3.6}$$

$$\underline{\underline{\varepsilon}}\, \underline{E} = \begin{bmatrix} \varepsilon_{NN} & \varepsilon_{N\perp} \\ -\varepsilon_{N\perp} & \varepsilon_{NN} \end{bmatrix} \begin{bmatrix} E_N \\ E_\perp \end{bmatrix} + \mu \left(\text{rot } \underline{E} - \underline{e}_\parallel \cdot \text{rot } \underline{E} \right) \tag{3.7}$$

where

$$\begin{cases} \varepsilon_{NN} = \dfrac{\omega^2}{c^2} S = \dfrac{\omega^2}{c_A^2} \displaystyle\sum_i \dfrac{f_i}{1 - \omega^2/\omega_{ci}^2} \\[2ex] \varepsilon_{N\perp} = i \dfrac{\omega^2}{c^2} D = i \dfrac{\omega^2}{c_A^2} \displaystyle\sum_i \dfrac{f_i\, \omega/\omega_{ci}}{1 - \omega^2/\omega_{ci}^2} \\[2ex] \mu = \dfrac{\underline{j}_o \cdot \underline{B}_o}{B_o^2} \\[2ex] c_A^2 = B_o^2 \Big/ \displaystyle\sum_j n_j m_j \qquad \text{(Alfvén speed)} \\[2ex] f_i = n_i m_i \Big/ \displaystyle\sum_j n_j m_j \qquad \text{(summations over ion species)} \end{cases} \tag{3.8}$$

The first term of (3.7) is well known [3] but not the second which is due to the equilibrium current $\underline{j}_o$. It comes straighforward from the third term of (3.4a).

Notice that the dielectric tensor (3.7) has been obtained without any assumption concerning the geometry. Because of the force-free condition (3.2) it neglects any finite β effect. If (3.7) is applied to a finite β equilibrium, it corresponds to neglecting the diamagnetic equilibrium current $j_{o\perp}$.

III.2 Warm Plasma Model

If parallel temperture is taken into account (but still neglecting the perpendicular one, that is neglecting the ion Larmor radius), we can replace ε_{NN} and $\varepsilon_{N\perp}$ in (3.8) by:

$$\begin{cases} \varepsilon_{NN} = \dfrac{\omega^2}{c^2} \sum_i \dfrac{\omega_{pi}^2}{2|k_\parallel| v_{t\parallel i}\, \omega} \left(Z_{1i} + Z_{-1\,i} \right) \\ \varepsilon_{N\perp} = i \dfrac{\omega^2}{c^2} \sum_i \dfrac{\omega_{pi}^2}{2|k_\parallel| v_{t\parallel i}\, \omega} \left(Z_{1i} - Z_{-1i} \right) \\ Z_{\ell i} = Z\left(\dfrac{\omega - \ell\omega_{ci}}{|k_\parallel| v_{t\parallel i}} \right) \quad ; \quad Z(\xi) = e^{-\xi^2} \left(i\sqrt{\pi} - 2 \int_0^\xi e^{t^2} dt \right) ; \\ v_{t\parallel i} = \text{parallel thermal velocity of i-th ion species.} \end{cases} \tag{3.9}$$

Note that (3.9) is only approximate when there exists an inhomogeneity of $\underline{B}_o$ along $\underline{B}_o$: in this case $k_\parallel$ is a differential operator and $\underline{\underline{\varepsilon}}$ is formally an integral operator. For a toroidal plasma we shall approximate $k_\parallel$ in (3.9) by n/r, where n is the toroidal wavenumber and r is the distance to the axis of the torus.

III.3 Variational Form and Discretization Procedure

We apply the finite element scheme described in Chapter II: after multiplication of (3.6) with $\underset{\sim}{\overset{*}{E}}$, integration over the plasma volume Ω, integration by parts, we obtain the variational form:

$$\int_{\Omega} dV \left\{ \mathrm{rot}\,\tilde{\underline{E}} \cdot \mathrm{rot}\,\underline{E} - \mu \tilde{\underline{E}} \cdot \mathrm{rot}\,\underline{E} - \tilde{\underline{E}} \cdot \begin{pmatrix} \varepsilon_{NN} & \varepsilon_{N\perp} \\ -\varepsilon_{N\perp} & \varepsilon_{NN} \end{pmatrix} \underline{E} \right\} \tag{3.10}$$

$$- i\omega \int_{\partial\Omega} \underline{d\sigma} \cdot (\tilde{\underline{E}} \times \underline{B}) = 0 \quad , \quad \forall\, \tilde{\underline{E}} \, .$$

We explicate (3.10) in an axisymmetric geometry (see Fig. 1) and write it in magnetic coordinates (ψ,χ,ϕ) (Fig. 1). The surface term in (3.10) is connected to the vacuum solution (including antenna and shell) which we will not discuss here. (This part is technical only. The reader can refer to Ref. [9] for more details). We obtain a variational form for two variables which are the two components of the wave electric field E_N and $E_\perp$.

We formally obtain:

$$\mathcal{L}(E_N, E_\perp) = 0 \, . \tag{3.11}$$

We can proceed with the discretization scheme described in Chapter II. However, the problem of rf waves in cold plasma theory has a particularity: the equations are <u>singular</u> where the <u>perpendicular resonance</u> condition is met:

$$\varepsilon_{NN} - k_{\parallel}^2 = 0 \quad , \tag{3.12}$$

which is the dispersion relation for shear Alfvén waves. These points are very important because <u>resonance absorption</u> occurs there. One can show in 1-D geometry that the behaviour of the wave field around the singularity is

$$\begin{cases} E_N \sim 1/x \\ E_\perp \sim \ln|x| \end{cases} \tag{3.13}$$

where x is the distance to the resonance.

In 2-D geometry the problem is more complex since $k_\parallel$ is a differential operator along the magnetic surfaces ψ = const. (Fig. 1). This implies that <u>the perp. resonances occur along ψ = const. surfaces</u> [11,14,15].

The way to turn the signularities is to add an imaginary part δ to ε_{NN} ($\varepsilon_{NN} + i\delta$), and make lim $\delta \to 0$, with $\delta > 0$ to satisfy the causality principle (any physical damping is causal: collisional, cyclotron, etc.).

One can show that $\partial E_\perp / \partial\psi$ has the same singular behaviour as E_N, as (3.13) suggests. A good finite element method should reproduce this result. This is the basis of what has been called the "finite hybrid elements" [16]: instead of considering (3.11) as a functional of two variables, we consider it as a functional of the variables and their derivatives:

$$\mathcal{L}\left(E_N^{(1)}, E_\perp^{(1)}, \frac{\partial E_\perp^{(2)}}{\partial\psi}, \frac{\partial E_\perp^{(3)}}{\partial\chi}, \frac{\partial E_N^{(2)}}{\partial\chi} \right) = 0 , \qquad (3.14)$$

with the constraints

$$E_N^{(1)} = E_N^{(2)} , \quad E_\perp^{(1)} = E_\perp^{(2)} = E_\perp^{(3)} . \qquad (3.15)$$

The main idea is to choose different basis functions for $E_N^{(1)}$ and $E_N^{(2)}$, $E_\perp^{(1)}$, $E_\perp^{(2)}$ and $E_\perp^{(3)}$, such that $\partial E_\perp^{(2)}/\partial\psi$ can behave in the same way as $E_N^{(1)}$ on a single mesh cell. Such an approach is called "non-conforming, non-polluting". We have chosen the lowest order finite elements so that each term in (3.14) is constant on a mesh cell. For more details see Refs. [9,16]. We just retain here that the hybrid elements are <u>faster</u> to compute, <u>simpler</u> to programme and yield <u>better results</u> than the usual, regular ones.

The discretization procedure follows the same guidelines as in Chapter II: we subdivide the plasma volume into finite-size mesh cells (ψ_i, χ_j), construct the matrix A and the source vector $\underline{b}$ and solve $A\underline{v} = \underline{b}$.

The obtained algorithm has been computer-programmed. The numerical code has been named LION [9] and has been installed on JET. Other similar codes exist or are under development in the world [5,17,18].

III.4 An Application to ICRF in JET Plasmas

Some results of the LION code have already been published [9,11] or are submitted for publication. In this section we show an example of what can be obtained with our global wave approach based on the finite element method.

Let us consider a JET-plasma with the following parameters: B_o = 3.4 T, R_o = 3m, a = 1.25m, elongation 1.68, safety factor q_o = 1, q_a = 2.2, n_{eo} = 3.242 10^{19} m^{-3}, mixture of deuterium and hydrogen with n_H/ne = 30%. We select the frequency near to 42 MHz and study three different positions of the antenna: Low Field Side (LFS), High Field Side (HFS) and Top-Bottom (TB). The basic theories (Budden's model [1]) predict for LFS almost 100% reflection of the fast wave and for HFS almost 100% absorption in a "single-pass". The HFS antenna would apparently be the good choice in this case. However, let us consider how our global approach can modify this opinion.

Figure 3 shows the total power absorbed versus applied frequency as calculated with the LION code for the three antennae. (In all cases the amplitude of the rf antenna current is normalized to the same value, therefore the power shown in Fig. 3 is a measure of the resistive impedance of the antenna). For the LFS antenna we find sharp peaks that we identify as global eigenmodes of the fast wave. Notice that the main peaks (f = 41.35 MHz, 42.85 MHz) are surrounded by smaller "satellite" peaks. These peaks are a result of the mode coupling due to the toroidal geometry: the modes have the same radial "wavenumber" as the main peaks but different polodial "wavenumbers". See in Fig. 4 the wave field for a main peak (f = 42.85 MHz) and in fig. 5 for its "satellite" (f = 42.24 MHz). As expected the wave is reflected in the centre of the plasma column. The presence of so many global modes for LFS excitation makes the average coupling of the LFS antenna rather high.

The results for the HFS antenna look quite different (Fig. 3). No global mode is excited, and the coupling is very low. This surprising result is an effect of the toroidal geometry. The fast wave is evanescent near the plasma boundary due to the low density in these regions. However, it is more evanescent on the HFS than on the LFS. If we consider the 1-D dispersion relation of the fast wave and replace the parallel wavenumber by n/r, which is 2.4 times larger on the HFS than on the LFS, we see that the evanescence extends over

23 cm on the HFS and 1 cm on the LFS. The HFS evanescence reduces the wavefield amplitude by a factor of 6 and thus the total absorbed power by a factor of about 36 (since it is proportional to the wavefield squared). Hence the coupling is weak.

This can be visualized on a plot of the wavefield solution for the HFS case, f = 42 MHz (Fig. 6). In addition to the evanescence near the HFS edge of the plasma we discover the remarkable structure of the perpendicular ion-ion hybrid resonances in the central regions. They lie on magnetic surfaces, as was expected from analytical theory. Inspecting Fig. 6 more carefully we observe poloidal modulations of the wavefield along the perpendicular resonances. These modulations are tighter and tighter as the perpendicular resonance surface approaches the surface where $\omega = \omega_{cH}$, which is situated on the right-hand side of the resonant surfaces. We can explain this result in the following way: the antenna excites a fast magnetosonic wave which in its turn excites shear Alfvén waves at specific places in the plasma where the resonance condition ($\varepsilon_{NN} - k_{\parallel}^2 = 0$) is met. Since the shear Alfvén wave has its group velocity parallel to $\underline{B}_0$ all the power exciting it will be "imprisoned" on a magnetic surface: this is the physical reason why the perpendicular resonances lie on magnetic surfaces. The poloidal modulation of the wavefield along the resonances simply reflects the fact that the parallel wavelength of the shear Alfvén wave goes to zero as ω goes to ω_{ci}. Due to the finite poloidal magnetic field of the equilibrium, the parallel wavelength projects onto the poloidal plane.

Note that the magnetic structure of the perpendicular resonances is a consequence of the existence of the poloidal magnetic field (B_{op}). If we make B_{op} go to zero, we observe that the poloidal extension of the resonances shrinks and that they come closer and closer in the radial direction until they merge to yield a vertical resonance structure defined by $\varepsilon_{NN} - n^2/r^2 = 0$ [11].

The results of the TB antenna (Fig. 3) show that global modes are also excited and the coupling is rather good. Unfortunately, most of the power is absorbed near the plasma boundary just in front of the antenna (not shown).

To summarize these results, we have shown that our global approach can bring a new picture to the theory of rf heating. Firstly, the description of

global modes is possible. We have shown a striking example where it has drastic consequences on the coupling of the antenna and where it brings an answer totally opposite (however not in contradiction) to the "single-pass" theories. Secondly, the geometrical effects on the structure of the perpendicular resonances and the effect of the poloidal field have been analyzed.

Other results obtained with the LION code include the determination of the power deposition profiles. We have found [19] a relationship between the absorption coefficient as calculated from "single-pass" theories and the focusing of the power towards the centre of the plasma.

Acknowledgements

I wish to thank Dr. K. Appert for reading the manuscript. I also benefited from interaction with Drs. J. Vaclavik, R. Gruber, T. Hellsten and O. Sauter.

This work was partly supported by the Swiss National Science Foundation.

References

[1] K.G. Budden, Radio Waves in the Ionosphere (Cambridge University Press, 1961).

[2] V.L. Guinzburg, Propagation of Electromagnetic Waves in Plasma (Gordon and Breach, 1961).

[3] T.H. Stix, The Theory of Plasma Waves (McGraw-Hill, New York, 1962).

[4] G. Strang and G.J. Fix, An Analysis of the Finite Element Method (Prentice-Hall, Englewood Cliffs, 1973).

[5] K. Itoh, S.I. Itoh and A. Fukuyama, Nucl Fus. 24 (1984), 13.

[6] V.P. Bhatnagar, R. Koch, P. Geilfus, R. Kirkpatrick and R.R. Weynants, Nucl. Fus. 24 (1984), 955.

[7] R. Koch, V.P. Bhatnagar, A.M. Messian and D. Van Eester, Comput. Phys. Commun. 40 (1986), 1.

[8] M. Brambilla, Comput. Phys. Reports 4 (1986), 71.

[9] L. Villard, K. Appert, R. Gruber and J. Vaclavik, Comput. Phys. Reports 4 (1986), 95.

[10] C.K. Phillips, F.W. Perkins, D.Q. Hwang and D.G. Swanson, Comput. Phys. Commun. 40 (1986), 23.

[11] K. Appert, G. Collins, T. Hellsten, J. Vaclavik and L. Villard, Plasma Phys. Contr. Fus. 28 (1986), 133.

[12] K. Appert et al., Phys. Rev. Lett. 54 (1985), 1671.

[13] K. Appert, J. Vaclavik and L. Villard, Lecture Notes: An Introduction to the Theory of Alfvén Wave Heating, Lausanne Report LRP 238/84 (1984), CRPP, Lausanne, Switzerland.

[14] T. Hellsten and E. Tennfors, Physica Scripta 30 (1984), 341.

[15] E. Tennfors, Plasma Phys. Contr. Fus. 28 (1986), 1483.

[16] R. Gruber and J. Rappaz, Finite Element Methods in Linear Ideal Magnetohydrodynamics (Springer-Verlag, Berlin-Heidelberg, 1985).

[17] E.F. Jaeger, D.B. Batchelor, H. Weitzner and J.H. Whealton, Comput. Phys. Commun. 40 (1986), 33.

[18] D. Edery and H. Picq, Comput. Phys. Commun. 40 (1986), 95.

[19] T. Hellsten and L. Villard, Contributed paper presented at the 14th EPS Conf. on Controlled Fusion and Plasma Physics, Madrid, 1987.

TABLE I

Comparison between different models

Model	N_d	N_L	N_W	Waves described by the model
(1) cold $E_\parallel=0$	2	0	1	• Fast magnetosonic (F) (sometimes called "Alfvén compressional"). The "surface mode" is the 1st radial mode of F for m = -1 • Shear Alfvén (or ion cyclotron). Global Modes of the Alfvén Wave (GEAW) = ion cyclotron modes.
(2) cold $E_\parallel\neq0$	4	0	2	Same as (1) plus "Surface Quasi-Electrostatic Wave" (SQEW).
(3) warm $E_\parallel=0$	2	0	1	Same as (1)
(4) hot $E_\parallel=0$	4	2	2	Same as (1) plus Kinetic Alfvén (KA) or ion Bernstein (IB)
(5) hot $E_\parallel\neq0$	6	2	$3^{(*)}$	Same as (4) plus "Surface Quasi-Electrostatic Wave" (SQEW)

N_d = order of the 1-D differential equation

N_L = order of the expansion in Larmor radius ($k\,\rho_L$)

N_W = number of wave branches in k_x^2

(*) = the "third branch" is usually unphysical since $k\,\rho_L > 1$.

TABLE I (cont'd)

Comparison between different models

Model	Features of non-homogeneous plasmas	Absorption mechanisms
(1) cold $E_\parallel=0$	The shear Alfvén wave appears as a perpendicular resonance of the fast wave ($\varepsilon_{xx}-k_\parallel^2 = 0$) (Alfvén and ion-ion hybrid perpendicular resonances), where the wave equation is singular. Singularity removed by making $\varepsilon_{xx} + i\delta$ and $\lim \delta \to 0$.	Resonance absorption. Power absorbed at the resonances is independent of δ for small δ. $\omega = \omega_{ci}$ is not a singularity of the Eqs. In fact $E_+ = 0 \to$ no cyclotron damping.
(2) cold $E_\parallel\neq0$	The perpendicular resonances of (1) are replaced by mode conversion to the SQEW	Mode conversion between F and SQEW. The SQEW has a resonance at the "ion-ion hybrid Buchsbaum resonance" ($\varepsilon_{xx} = 0$).
(3) warm $E_\parallel=0$	Same as (1) unless the perpendicular resonance is close to ω_{ci}	Same as (1) plus ion cyclotron damping of F. (parallel temperature only)
(4) hot $E_\parallel=0$	The perpendicular resonances of (1) are replaced by mode conversion to the KA. Also mode conversion to the IB near $\omega=2\omega_{ci}$.	Ion cyclotron damping of the F, KA and IB at $\omega=\omega_{ci}$ and $\omega=2\omega_{ci}$. Mode conversion processes.
(5) hot $E_\parallel\neq0$	Same as (4) but if $c_A/v_{the} > 1$ mode conversion to the SQEW instead of Ka.	Same as (4) plus Landau damping and Transit Time Magnetic Pumping (TTMP).

TABLE II

Weights c_ℓ and abcissae ξ_ℓ for the Gaussian Integration Formula

$$\int_{-1}^{1} g(\xi)d\xi = \sum_{\ell=1}^{m} c_\ell g(\xi_\ell)$$

m	c_ℓ	ξ_ℓ
1	2	0
2	1	$\pm$ 1/3
3	8/9 5/9	0 $\pm$ 0.774597
4	0.642145 0.347855	$\pm$ 0.339981 $\pm$ 0.861136

Figure Captions

Fig. 1: Toroidal configuration showing the local magnetic frame of reference ($\underline{e}_N$, $\underline{e}_\perp$, $\underline{e}_\parallel$), the polar coordinates (r,z,ϕ) and the toroidal magnetic coordinates (ψ,χ,ϕ).

Fig. 2: Piecewise linear approximation $E_h(x)$ of $E(x)$ with linear basis functions $\phi_i(x)$.

Fig. 3: Total resistive power (arbitrary units) versus frequency for a JET plasma containing deuterium and 30% hydrogen excited with three different types of anntennae: LFS, HFS and TB. Only the contribution of the toroidal wavenumber n = -15 is represented.

Fig. 4: Level lines of the wavefield E for the LFS case, f = 42.85 MHz, corresponding to a main peak of Fig. 3.

Fig. 5: Level lines of the wavefield E for the LFS case, f = 42.24 MHz, corresponding to a satellite peak of Fig. 3.

Fig. 6: Level lines of the wavefield E for the HFS case, f = 42 MHz.

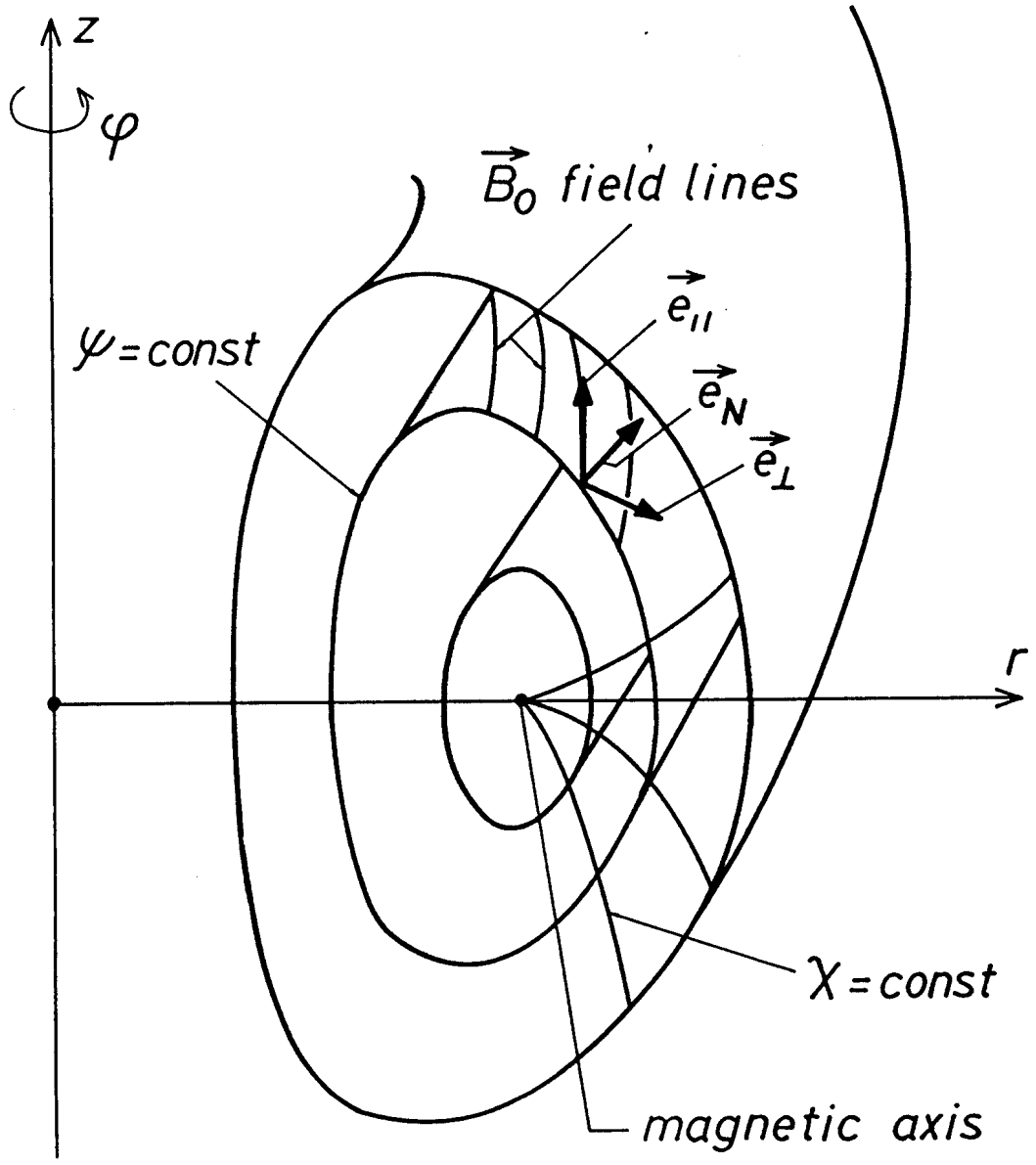
z
φ
$\vec{B}_0$ field lines
$\vec{e}_{\parallel}$
$\vec{e}_N$
$\vec{e}_\perp$
ψ = const
r
χ = const
magnetic axis

FIG. 1

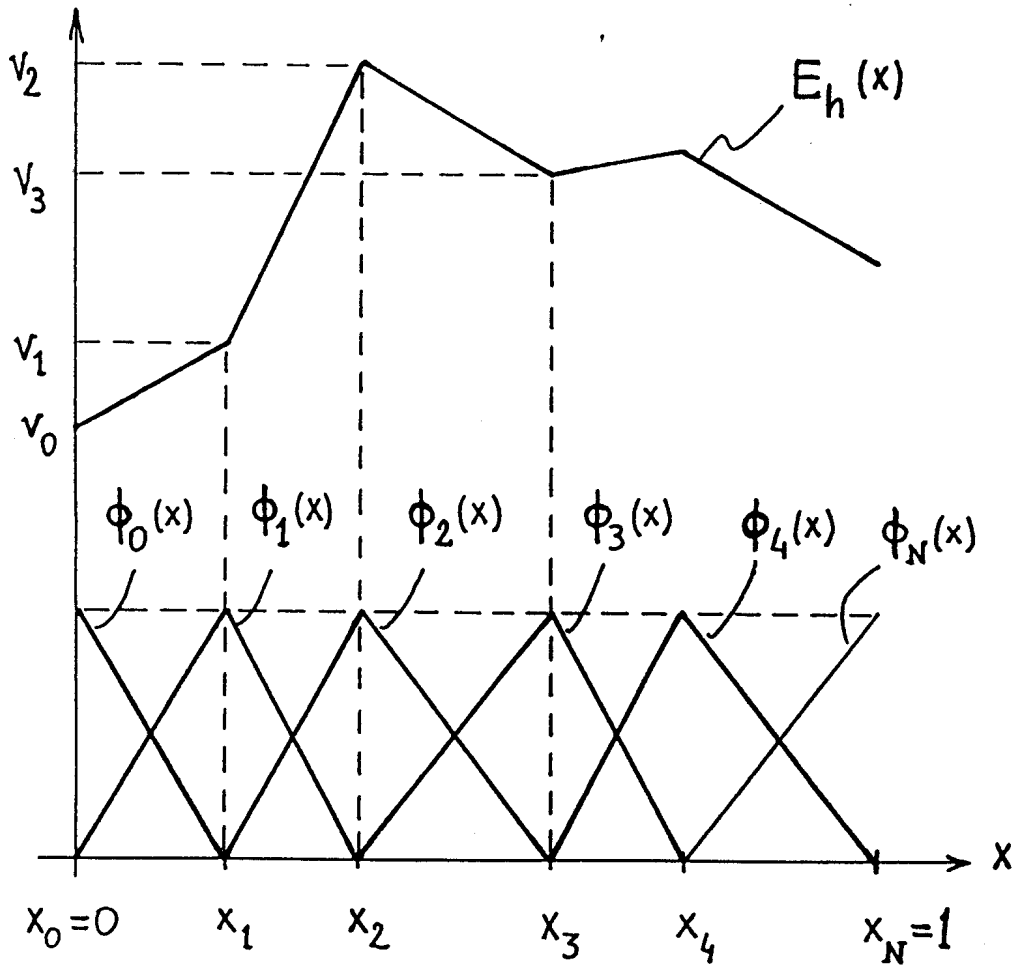
v_2
v_3
v_1
v_0
$E_h(x)$
$\phi_0(x)$
$\phi_1(x)$
$\phi_2(x)$
$\phi_3(x)$
$\phi_4(x)$
$\phi_N(x)$
x
$x_0=0$
x_1
x_2
x_3
x_4
$x_N=1$

FIG. 2

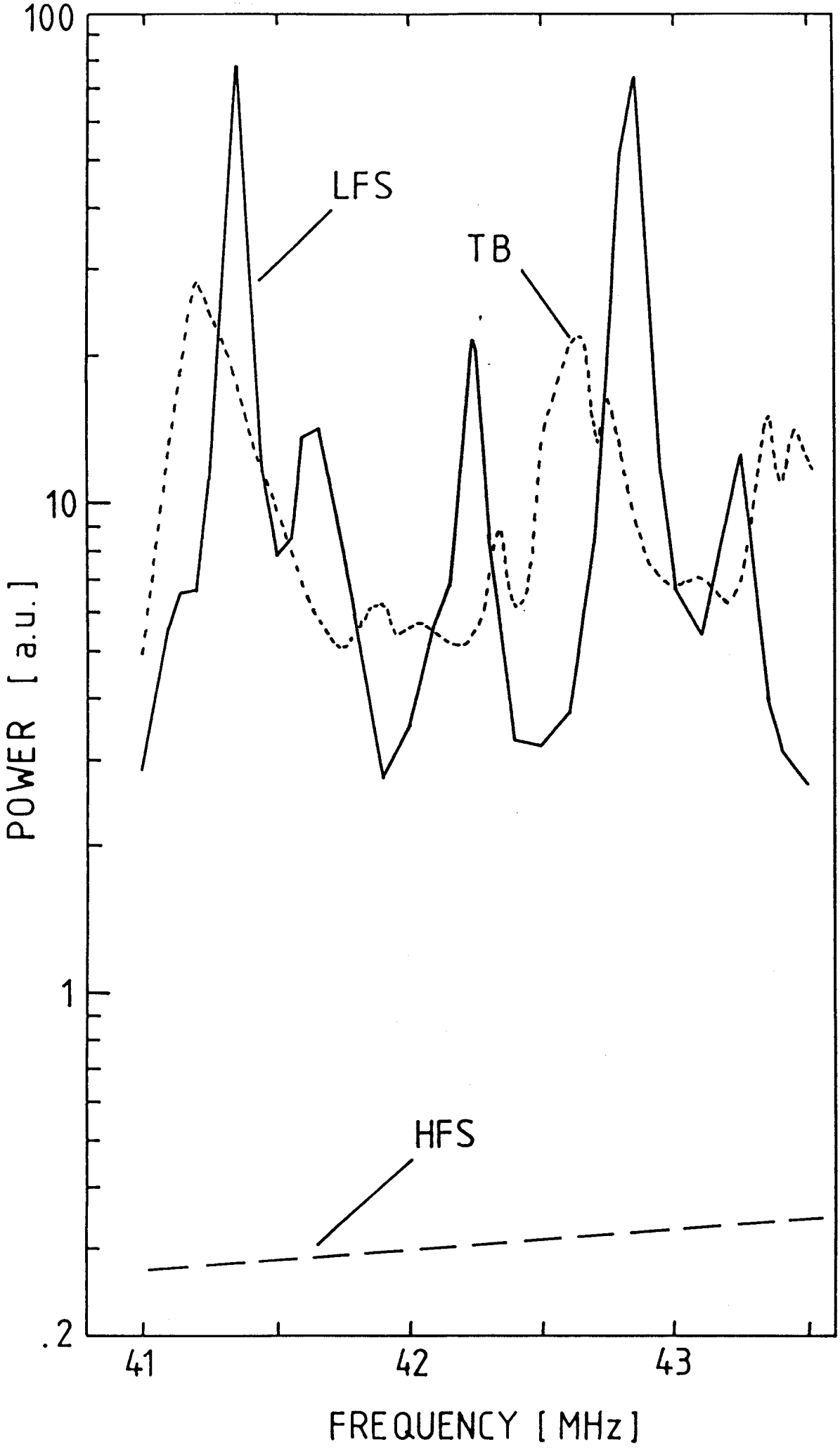

FIG. 3

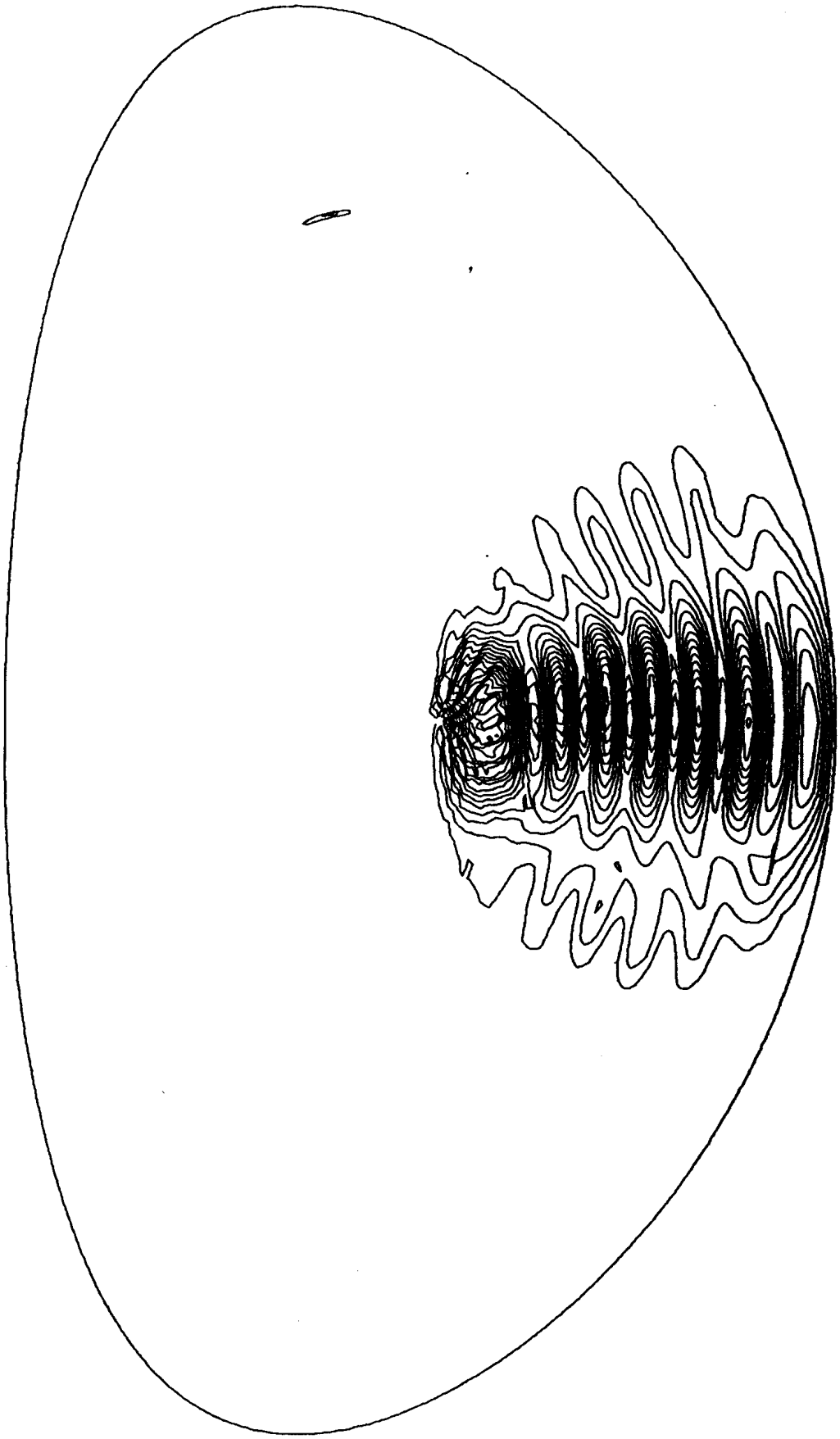

FIG. 4

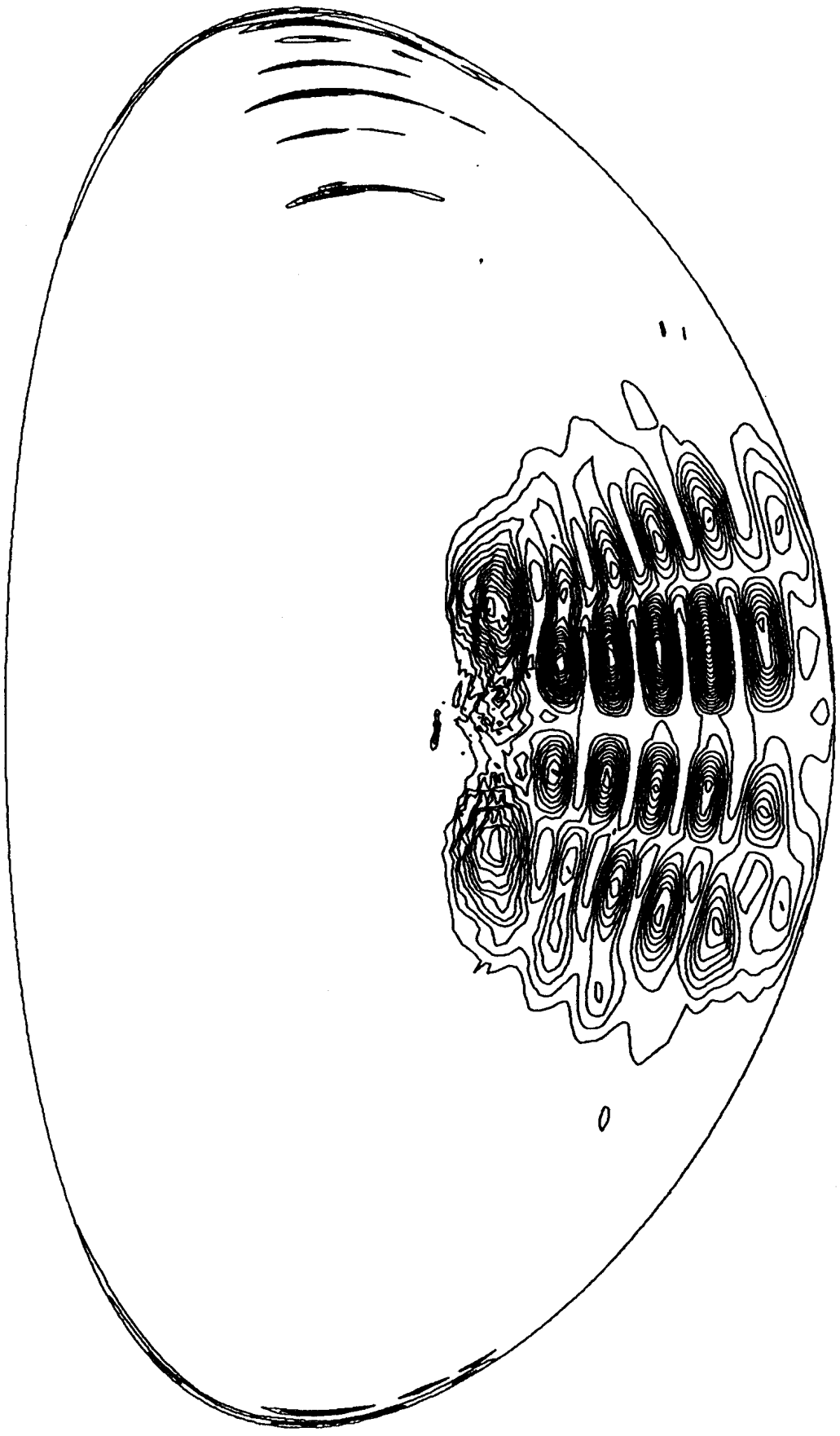

FIG. 5

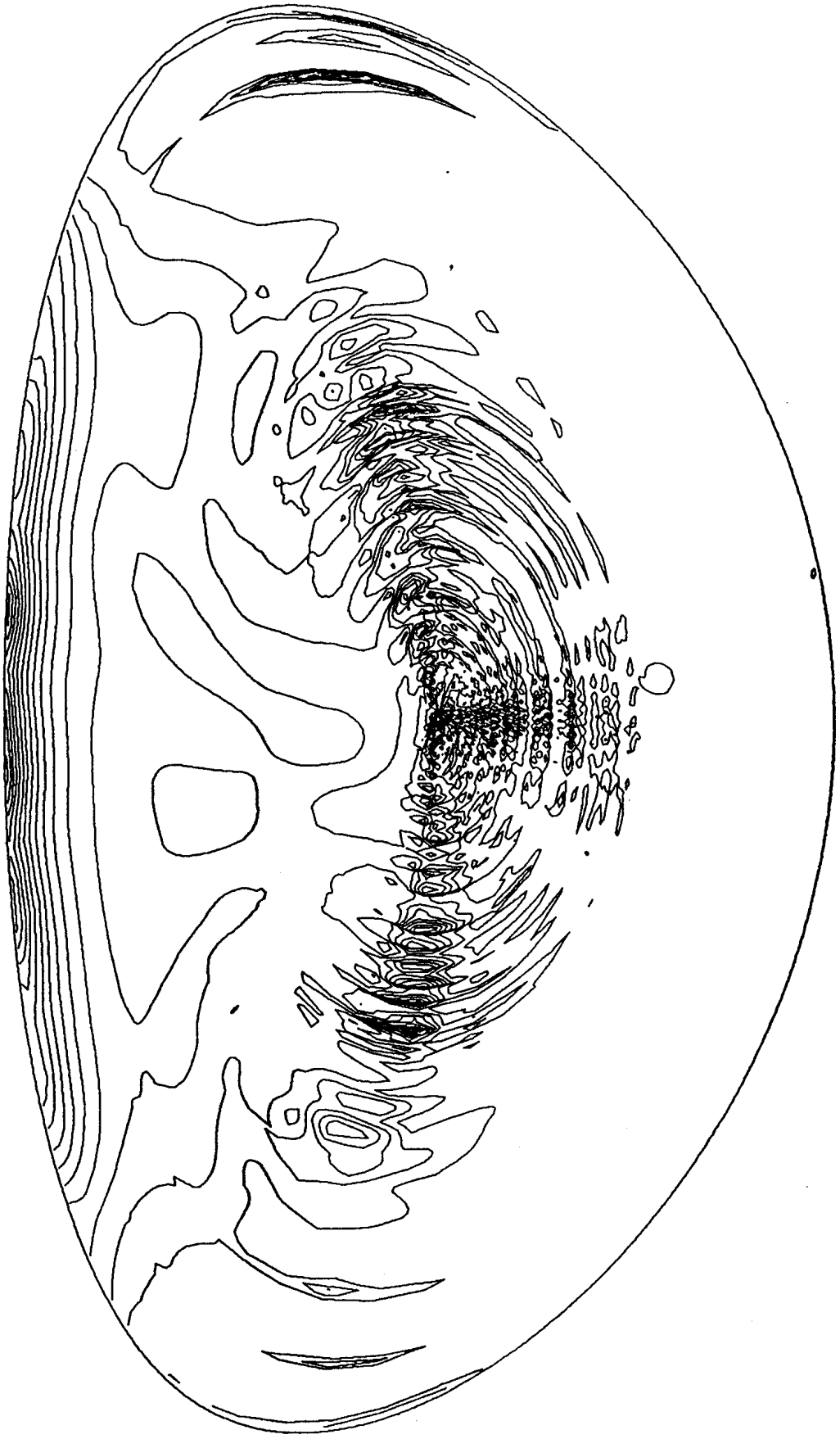

FIG. 6

EXTERNAL KINK IMPOSED OPERATING BOUNDARIES IN TOKAMAKS

W.A. Cooper, F. Yasseen, F. Troyon, T. Tsunematsu* and A.D. Turnbull+

Centre de Recherches en Physique des Plasmas, Association Euratom-Confédération Suisse, Ecole Polytechnique Fédérale de Lausanne, 21, Av. des Bains, CH-1007 Lausanne, Switzerland

ABSTRACT

The linear stability code ERATO is applied to MHD equilibria of low and moderate aspect ractio to determine the operational diagrams imposed by n = 1 external kink modes in the q_o-q_s domain. An unstable wedge between two stable windows appears at low aspect ratio, where strong non-resonant m = 1 instabilities are driven by toroidal coupling effects.

INTRODUCTION

Ideal magnetohydrodynamic (MHD) theory constitutes the simplest model to describe the dynamics of magnetic plasma confinement systems. Nonetheless, the very simplicity of the dynamics permits this model to tackle problems in devices with very complicated geometries. Linear MHD stability codes such as PEST[1] and ERATO[2] have become very important tools in the design of Tokamaks. They help map out the regions of stable operation and identify those configurations that maximise the parameter beta (β) which is the ratio of the volume average pressure to the volume average magnetic field energy density.

We briefly describe the ERATO stability code and discuss the input profiles that are used to generate MHD equilibria. The domains of stable operation imposed by n = 1 external kink modes for Tokamaks with low and moderate aspect ratios are compared. The eigenstructure patterns of unstable equilibria with similar values of β and safety factor profiles in each one of these domains are also investigated.

* Permanent Address: Japanese Atomic Energy Research Institute (JAERI), Tokai, Japan.

+ Permanent Address: GA Technologies, Inc., La Jolla, CA / U.S.A.

PHYSICS BACKGROUND OF ERATO

The ERATO code determines the linear ideal MHD stability properties of axisymmetric plasma configurations by examining the energy principle[3] that is obtained from the linearised MHD equations, namely,

$$\delta L = \delta W_P + \delta W_V - \omega^2 \delta W_K = 0. \qquad (1)$$

The potential energy of the plasma is expressed as (2)

$$\delta W_P = \tfrac{1}{2} \int d^3x \left\{ \left[\underline{\nabla} \times (\underline{\xi} \times \underline{B}) + (\underline{\nu} \cdot \underline{\xi})(\underline{j} \times \underline{\xi}) \right]^2 + \gamma p (\underline{\nabla} \cdot \underline{\xi})^2 - 2(\underline{\nu} \cdot \underline{\xi})^2 (\underline{j} \times \underline{\nu}) \cdot (\underline{B} \cdot \underline{\nabla}) \underline{\nu} \right\}, \qquad (2)$$

where $\underline{\nu} \equiv \underline{\nabla}\phi / |\underline{\nabla}\phi|$ is the unit vector normal to the flux surfaces. The equilibrium magnetic and current density fields are $\underline{B}$ and $\underline{j}$, respectively, and the perturbed displacement vector is $\underline{\xi}$. The equilibrium plasma pressure is p and γ is the adiabatic index. The contribution of the vacuum fields to the energy of the system is given by

$$\delta W_V = \frac{1}{2} \int d^3x \left(\underline{\nabla} \times \underline{A} \right)^2, \qquad (3)$$

where $\underline{A}$ is the perturbed magnetic vector potential, and the kinetic energy of the system is

$$\delta W_K = \frac{1}{2} \int d^3x \, \rho \xi^2, \qquad (4)$$

where ρ is the mass density. A plasma equilibrium state is unstable if the eigenvalue $\omega^2 > 0$. The value obtained for ω corresponds to the growth rate of the instability.

Furthermore, the perturbation is expanded as[4]

$$\underline{\xi} = \underline{\eta}(\psi, \theta) \exp\left[in(\phi - q\theta) \right] \qquad (5)$$

when $nq > 10$, where ϕ is the geometric toroidal angle and θ is the poloidal angle in a straight magnetic field line coordinate system (ψ, θ, ϕ). In systems with axisymmety, instabilities with different

different toroidal mode numbers n are decoupled one from another and can be therefore investigated independently. The safety factor q, which is the derivative of the toroidal magnetic flux with respect to the poloidal magnetic flux, corresponds to the number of toroidal transits a magnetic field line makes per poloidal transit. This quantity is one of the critical variables of Tokamak MHD stability analysis because instabilities tend to concentrate in regions where q has an integer value. To increase the accuracy of the calculations, the ERATO code is constructed with a variable radial mesh that permits packing around the rational q surfaces. The perturbed vector amplitudes $\underline{\eta}(\psi,\theta)$ are expanded further using finite hybrid elements. A detailed description of the numerical scheme of the ERATO code can be found in Reference 2.

PARAMETRISATION OF THE EQUILIBRIA

The plasma-vacuum interface for the MHD equilibrium models under consideration is described by

$$r = R + a\cos(\theta + \delta\sin\theta) \tag{6}$$

and

$$z = E a \sin\theta \,, \tag{7}$$

where r is the distance of any boundary point from the major axis and z is its distance from the midplane. The other parameters are the major radius R, the minor radius a, the elongation E and the triangularity δ.

The average toroidal current density flowing within a poloidal magnetic flux surface ψ is defined as

$$J(\psi) = \frac{2\pi}{V'} \int_0^{2\pi} d\theta \sqrt{g}\,(\underline{j}\cdot\nabla\phi) \,, \tag{8}$$

where $V'(\psi) \equiv 2\pi \int_0^{2\pi} d\theta\sqrt{g}$ is the differential volume and $\sqrt{g}$ is the Jacobian of the transformation from the cylindrical coordinates

(r,ϕ,z) to the magnetic coordinates (ψ,θ,ϕ). The prime indicates the derivative of a flux surface quantity with respect to ψ. The total current is

$$I = \frac{1}{2\pi}\int_{\psi_0}^{\psi_s} d\psi\, V'(\psi)\, J(\psi). \tag{9}$$

We prescribe the $p'(\psi)$ and $J(\psi)$ profiles with functional forms that have continuous piecewise smooth radial derivatives, namely

$$p'(\psi) = \begin{cases} 0 & \psi_o \le \psi < \psi_c \\ \text{cubic function} & \psi_c \le \psi < \psi_d \\ \text{quadratic function} & \psi_d \le \psi \le \psi_s \end{cases} \tag{10}$$

and

$$J(\psi) = \begin{cases} \text{quadratic function} & \psi_o \le \psi < \psi_a \\ \text{cubic function} & \psi_a \le \psi < \psi_b \\ 0 & \psi_b \le \psi \le \psi_s \end{cases} \tag{11}$$

Typically we choose $p'(\psi_s) = 0$, $p'(\psi_d)$ to be a maximum, and $\psi_d = \psi_b$ so that the peak of the pressure gradient matches the point at which J vanishes. A detailed description of the specific forms and the philosophy behind the choice of these profiles can be found in Reference 5.

NUMERICAL RESULTS

We concentrate here on a configuration with low aspect ratio. Although design and engineering constraints pose some severe problems, the physics aspects indicate the possibility of operating at very high values of β which makes this an attractive type of device to consider.[6] The plasma boundary parameters are given by E = 1.68, A ≡ R/a = 1.67 and δ = 0.3. The operational diagram in the q_o-q_s space determined by n = 1 external kink instabilities is obtained with fixed $\beta_I = 8\pi\int p\,ds/\mu_0 I^2 = 0.35$ and shown in Fig. 1. The q_o-q_s

domain is scanned by varying the current, the current profile and the total pressure. What we find for $q_S < 4$ are two stable bands localised about $q_O = 1.0$ and $q_O = 1.1$, with an unstable band wedged in between. This type of structure differs considerably from that obtained in a more conventional Tokamak with moderate aspect ratio. As an illustration, we consider a configuration with A = 3.7, E = 2.0 and $\delta = 0.4$. The corresponding operational diagram that is shown in Fig. 2 for a case with $\beta_I = 0.95$ has only a single stable band. It is also useful to compare the eigenstructures of two unstable equilibria that lie in the operating diagrams presented and have similar monotonic q profiles and β values. The instability flow pattern for an A = 1.67 equilibrium that lies in the unstable wedge of Fig. 1 with $q_O = 1.065$, $q_S = 3.517$ and $\beta = 8\%$ appears in Fig. 3. The pattern reveals noticeable m = 2 and m = 3 activity about the q = 2 and q = 3 surfaces, respectively. Throughout the bulk of the plasma a significant non-resonant m = 1 structure is clearly visible that is driven unstable by the strong toroidal coupling with the m = 2 and m = 3 external modes at this low aspect ratio. The instability flow pattern for an A = 3.7 equilibrium with $q_O = 1.06$, $q_S = 2.89$ and $\beta = 7.4\%$ appears in Fig. 4. A dominant external m = 2 mode is localised about the q = 2 surface. Here a non-resonant m = 1 mode is also apparent, but it is much weaker than the one shown in Fig. 3 because the toroidal coupling effects at A = 3.7 are not as strong.

SUMMARY AND DISCUSSION

A brief description of the ERATO stability code has been presented and the profiles and boundaries that are used to prescribe MHD equilibria have been discussed. We choose to employ $J(\psi)$ as the input profile in order to have control over the total plasma current and the current profile as well as to avoid peeling instabilities that arise from current density discontinuities at the plasma-vacuum interface when for example the $q(\psi)$ profile is prescribed and maintained in a flux conserving manner.

We have examined the stability of a low aspect ratio configura-

tion to n = 1 external kink modes and found that they were two stable operating windows with an unstable wedge in between localised near q_o = 1.05 in the q_o - q_s domain. In a more conventional moderate aspect ratio configuration, only a single stable operating band is observed in this domain. The eigenstructure in a low A equilibrium in the unstable wedge has significant non-resonant m = 1 activity throughout the bulk of the plasma driven by the strong toroidal coupling with m > 2 instabilities. A comparable moderate A unstable equilibrium displays negligible non-resonant m = 1 activity because the toroidal coupling effects with the dominant m > 2 modes is correspondingly weaker. These equilibria we have computed are not optimal for ballooning stability. However, because the low n-kink modes tend to be sensitive to the plasma current, the current profile and the global value of β, but relatively independent of the details of the pressure profile, the stability to ballooning modes can be achieved with appropriate retailoring of the p' profile without significantly altering the kink mode stability properties of the configurations under consideration.

REFERENCES

[1] R.C. Grimm, J.M. Greene and J.L. Johnson, Methods of Computational Physics, Vol. 16, Ch. 4, Academic Press.

[2] R. Gruber, F. Troyon, D. Berger, L.C. Bernard, S. Rousset, R. Schreiber, W. Kerner and K.V. Roberts, Comp. Phys. Commun. 21, 323 (1981).

[3] I.B. Bernstein, E.A. Frieman, M.D. Kruskal and R.B. Kulsrud, Proc. Royal Soc. A17, 244 (1958).

[4] R. Gruber, F. Troyon and T. Tsunematsu, Plasma Phys. 25, 207 (1983).

[5] A.D. Turnbull, M.A. Secrétan, F. Troyon, S. Semenzato and R. Gruber, J. Comput. Phys. 66, 391 (1986).

[6] S.G. Bespoludennov, L.M. Degtyarev and S.Yu. Medvedev, Sov. J. Plasma Phys. 12, 441 (1986).

FIGURE CAPTIONS

Fig. 1: The β_I = 0.35 stability boundaries with q_o - q_s space for a configuration with A = 1.67, E = 1.68 and δ = 0.3 (solid curve). The dashed lines connect points of constant normalised current $\mu_0 I/RB_o$.

Fig. 2: The β_I = 0.95 stability boundaries in the q_o - q_s space for a configuration with A = 3.7, E = 2.0 and δ = 0.4 (solid curve). The dashed lines connect point of constant normalised current.

Fig. 3: The instability flow pattern in a configuration with A = 1.67, E = 1.68, δ = 0.3 and β = 8%. The equilibrium state has q_o = 1.065 and q_s = 3.517.

Fig. 4: The instability flow pattern in a configuration with A = 3.7, E = 2.0, δ = 0.4 and β = 7.4%. The equilibrium state has q_o = 1.06 and q_s = 2.89.

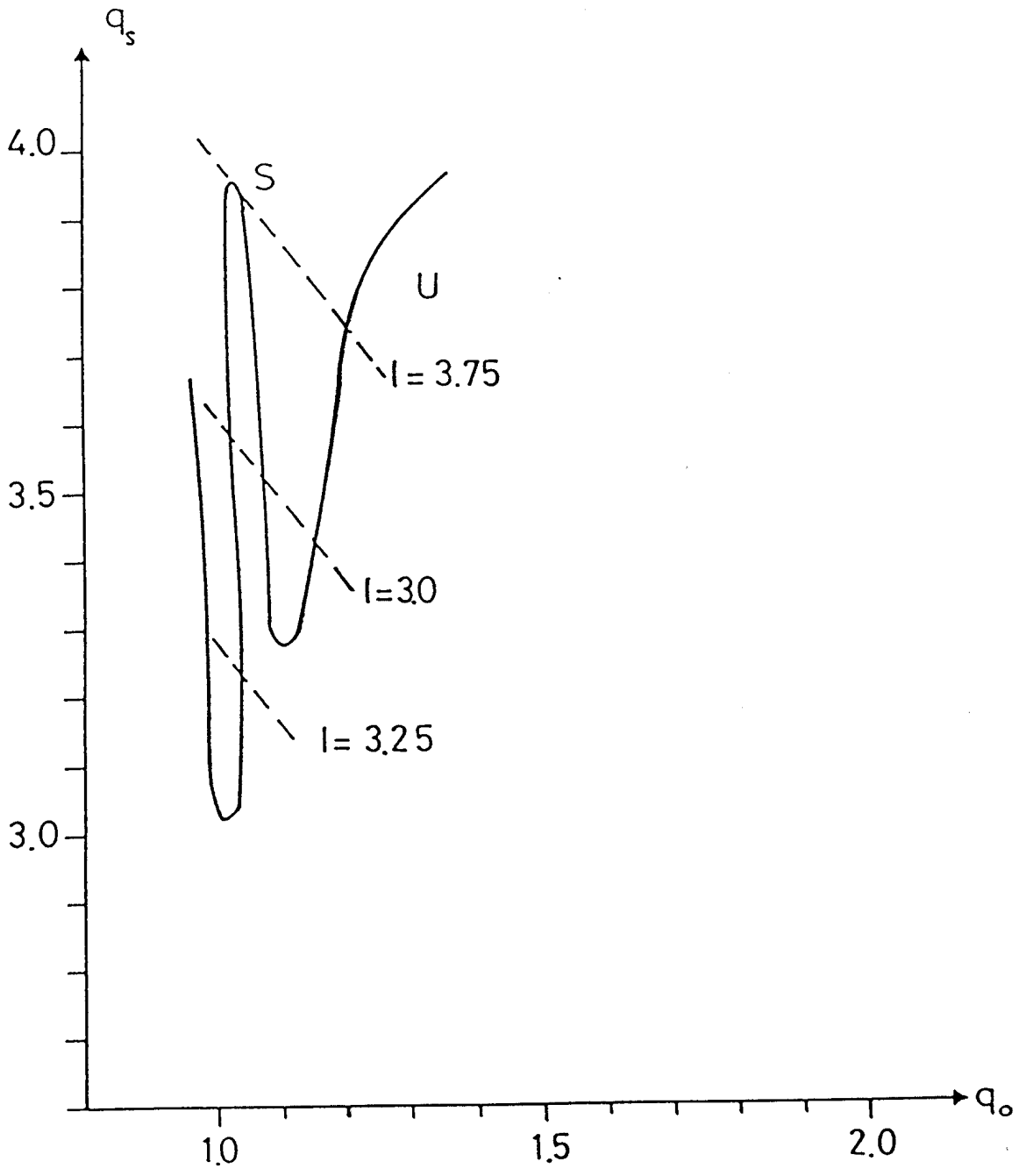

FIG. 1

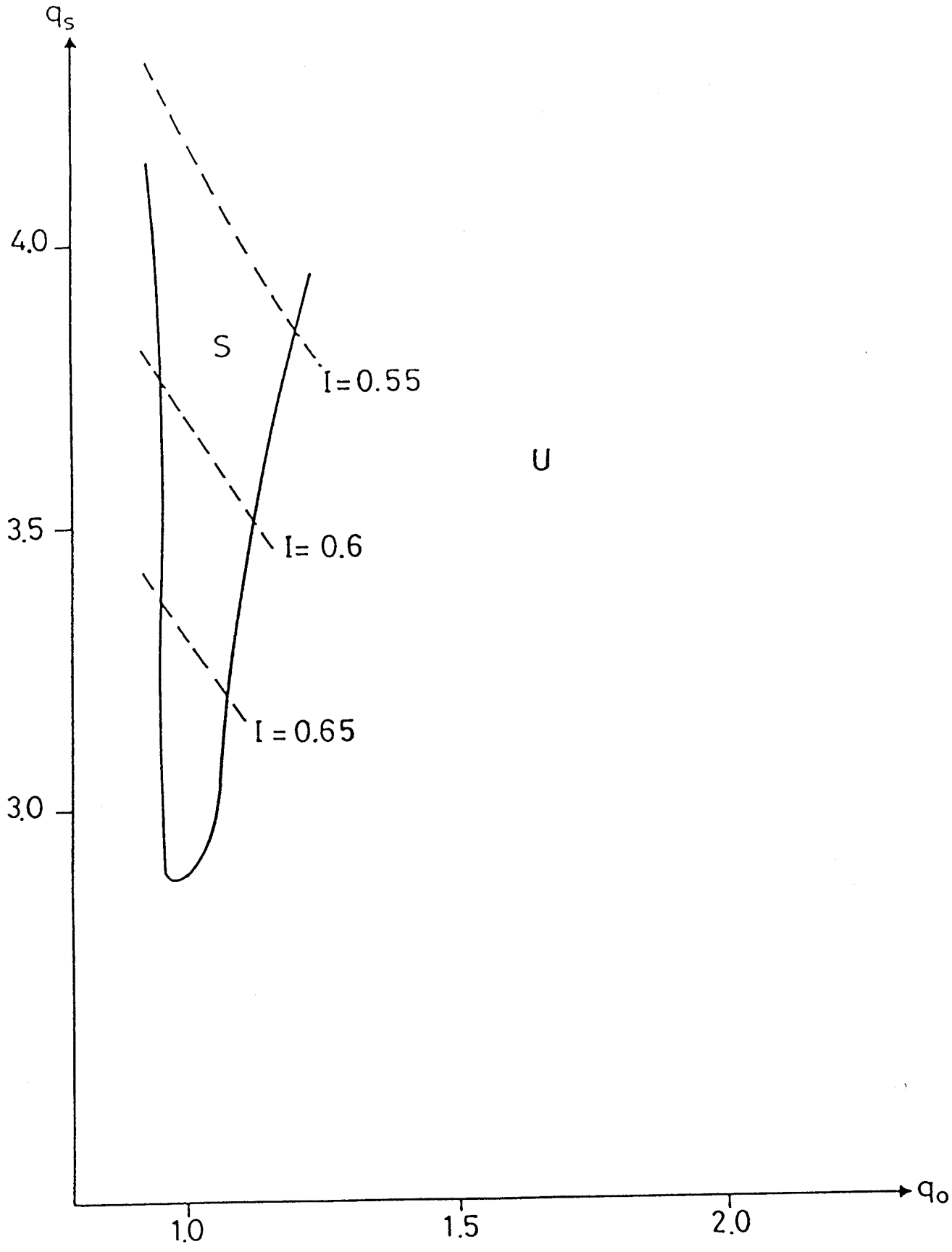

FIG. 2

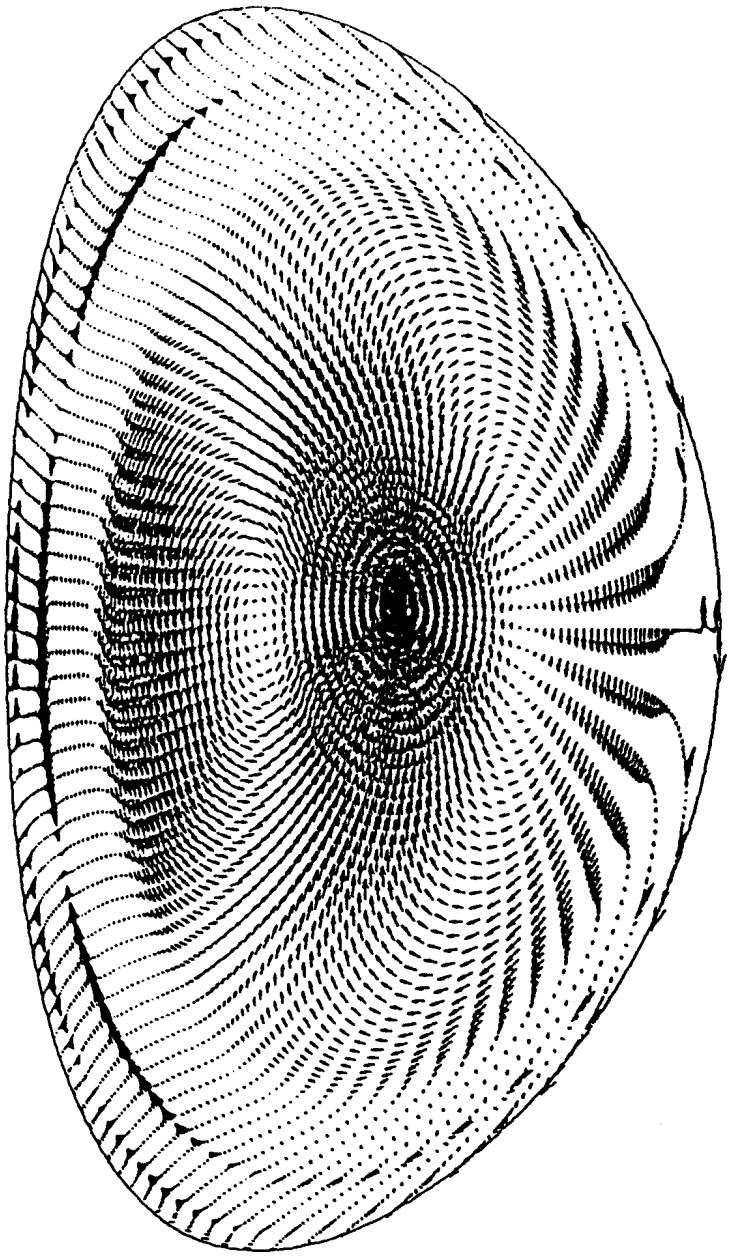

FIG. 3

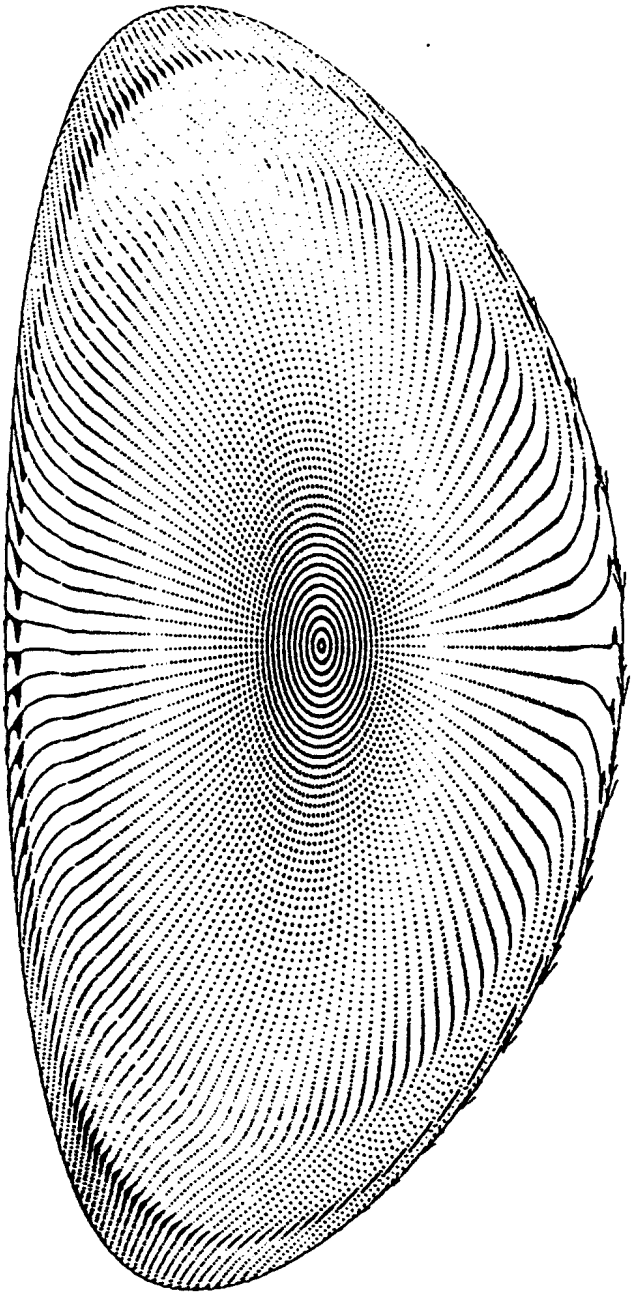

FIG. 4